

1 Strong neutral sweeps occurring during a population contraction

2

3 Antoine Moinet^{1,2,3}, Stephan Peischl*^{1,2} and Laurent Excoffier*^{2,3}

4

5 1. Interfaculty Bioinformatics Unit, University of Bern, Baltzerstrasse 6, 3012 Bern,
6 Switzerland;

7 2. Swiss Institute of Bioinformatics, 1015 Lausanne, Switzerland;

8 3. Institute of Ecology and Evolution, University of Bern, Baltzerstrasse 6, 3012 Bern,
9 Switzerland;

10 Abstract

11 A strong reduction in diversity around a specific locus is often interpreted as a recent rapid
12 fixation of a positively selected allele, a phenomenon called a selective sweep. Rapid fixation of
13 neutral variants can however lead to similar reduction in local diversity, especially when the
14 population experiences changes in population size, e.g., bottlenecks or range expansions. The
15 fact that demographic processes can lead to signals of nucleotide diversity very similar to
16 signals of selective sweeps is at the core of an ongoing discussion about the roles of
17 demography and natural selection in shaping patterns of neutral variation. Here we
18 quantitatively investigate the shape of such neutral valleys of diversity under a simple model of
19 a single population size change, and we compare it to signals of a selective sweep. We
20 analytically describe the expected shape of such “neutral sweeps” and show that selective
21 sweep valleys of diversity are, for the same fixation time, wider than neutral valleys. On the
22 other hand, it is always possible to parametrize our model to find a neutral valley that has the
23 same width as a given selected valley. We apply our framework to the case of a putative
24 selective sweep signal around the gene *Quetzalcoat1* in *D. melanogaster* and show that the
25 valley of diversity in the vicinity of this gene is compatible with a short bottleneck scenario
26 without selection. Our findings provide further insight in how simple demographic models can
27 create valleys of genetic diversity that may falsely be attributed to positive selection.

28 Introduction

29 Past demography and natural selection play a critical role in shaping extant genetic diversity. A
30 central question in population genetics is to quantify their respective impact on observed
31 genomic diversity. Because selection interferes with demographic estimates and vice versa,
32 estimation of one of these two components is difficult without accounting for the other
33 (Charlesworth *et al.* 1993, 1995; Kaiser and Charlesworth 2009; O'Fallon *et al.* 2010;
34 Charlesworth 2013; Nicolaisen and Desai 2013; Johri *et al.* 2020, 2021b). Moreover, the relative
35 importance of demography and selection as determinants of genome wide diversity is currently
36 hotly debated, and may vary extensively among species (Corbett-Detig *et al.* 2015; Rousselle *et*
37 *al.* 2018; Pouyet and Gilbert 2019; Galtier and Rousselle 2020). It has been shown that selection
38 and demography can leave very similar footprints on the genetic diversity of a population
39 (Andolfatto and Przeworski 2000; Teshima *et al.* 2006; Thornton and Jensen 2007; Johri *et al.*
40 2021a). Disentangling the effects of demography and selection is therefore crucial to avoid
41 erroneous inference of evolutionary scenarios from genomic data (Jensen *et al.* 2005; Wares
42 2009; Mathew and Jensen 2015; Johri *et al.* 2020).

43 Hard selective sweeps lead to valleys of strongly reduced diversity around positively selected
44 sites due to the hitchhiking of linked neutral loci (Maynard Smith and Haigh 1974), such
45 observations of strong depletions of diversity in some genomic regions are often interpreted as
46 due to past episode of positive selection, because the probability to observe a fast fixation of a
47 neutral variant in a population of constant size is extremely low. However, during a range
48 expansion for instance, some neutral or even mildly deleterious mutations can go quickly to
49 fixation due to the low effective size of populations on the front of the range (Edmonds *et al.*
50 2004; Klopstein *et al.* 2006; Hallatschek and Nelson 2008; Peischl *et al.* 2013), a phenomenon
51 termed allele surfing (Klopstein *et al.* 2006). Theoretical studies have shown that the average
52 neutral diversity on the wave front decays exponentially as the range expands (Hallatschek and
53 Nelson 2008), similarly to what happens when a population experiences a sudden decay of the
54 population size, i.e. a population contraction, due to a drastic change in the environment for
55 example. In both cases, a mutation appearing when the population size is shrinking might go
56 quickly to fixation, inducing a strong decrease of diversity in the surrounding genomic region,

57 whereas the average level of diversity might stay quite high depending on the strength and the
58 duration of the contraction. As a result, the coalescent tree of alleles sampled in a population
59 with strongly reduced effective population size will have short external branches, and long
60 internal branches, depending on the parameters of the model (Excoffier *et al.* 2009). The site
61 frequency spectrum associated to such a tree resembles a neutral SFS, but with a lack of rare
62 alleles and an excess of high frequency sites, i.e. it becomes “flatter” (Sousa *et al.* 2014; Peischl
63 and Excoffier 2015). The footprint left by the rapid fixation of a neutral allele on the
64 surrounding genomic diversity, might thus be like that of a positively selected allele sweeping
65 through a constant size population.

66 The expected shape of nucleotide diversity in genomic regions surrounding a site undergoing a
67 rapid neutral fixation has been investigated analytically and numerically. Tajima (1990) studied
68 the reduction of diversity during a neutral fixation at a given recombination distance from the
69 fixing site. His results rely on rigorous mathematical arguments based on diffusion theory, but
70 no closed form solution is provided for the shape of a neutral sweep. Johri *et al.* (2021a)
71 described the valley of diversity occurring around a neutral fixation using an approach
72 introduced for selective sweeps, assuming that the evolution of the allele frequency is that of a
73 selected allele except in the initial stochastic phase. Here, we extend this work by inferring the
74 dynamics of fixation of neutral alleles after a population contraction and we examine their
75 effects on neighboring regions of the genome. We provide an analytical result for the expected
76 coalescence time as a function of the recombination distance from the locus undergoing a fast
77 fixation. Importantly, our results apply regardless of the process driving the allele going to
78 fixation (neutrality, positive selection, background selection), as it only relies on the typical
79 trajectory of an allele going to fixation in a given time, even though this trajectory differs
80 depending on the underlying driver of this fixation (i.e., neutrality or selection). We compare
81 our results against simulations and find that they hold for a wide range of realistic parameter
82 combinations. We compare our results about the signature of neutral sweeps to patterns
83 expected under selective sweeps and discuss potential differences between the signatures that
84 could potentially allow us to discriminate between neutral and selective processes for a given
85 demographic scenario. Finally, we investigate the similarity between the genomic signature of

86 an allele going to fixation either selectively or neutrally and observe that a selective sweep
87 signal can in principle be replicated in a neutral model with an appropriate choice of
88 demographic parameters. To illustrate this point, we examine a classical example of a selective
89 sweep found in the genome of *D. melanogaster* around the *Qtz1* gene (Rogers *et al.* 2010). We
90 conclude that strong diversity depletions in the genome of a population, often attributed to the
91 effect of positive selection, can be obtained with demographic effects only, and we call for
92 caution when trying to detect signals of adaptation from genomic data, adding support to
93 previous studies reaching similar conclusions (Thornton and Jensen 2007; Crisci *et al.* 2013;
94 Jensen *et al.* 2019).

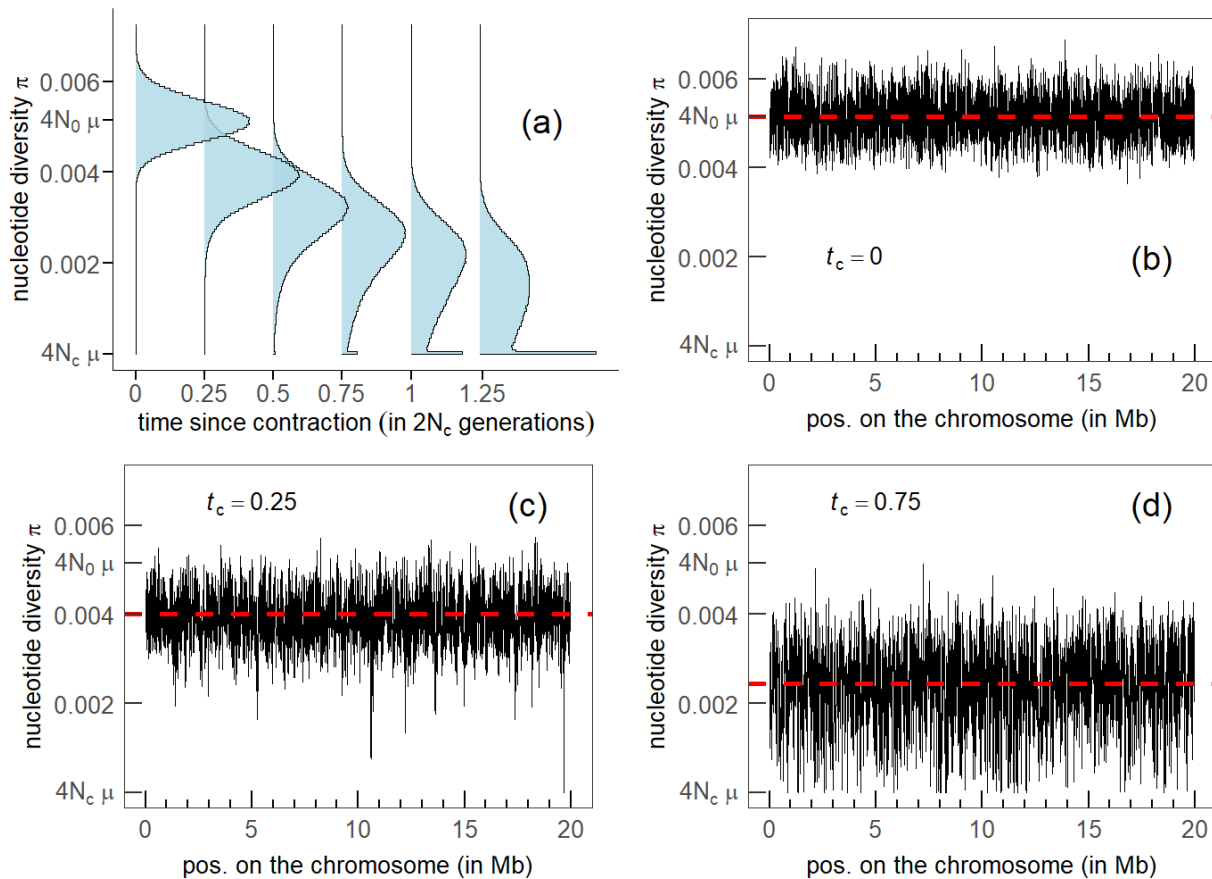
95 Model

96 We model here the effect of an instantaneous population contraction on genomic diversity.
97 Throughout the whole manuscript, time is measured backwards. We assume that t_c generations
98 before the present, the population size instantaneously dropped from N_0 diploid individuals to
99 N_c individuals with $N_c < N_0$. We assume a standard coalescent model (Kingman 1982a; b) with
100 discrete non-overlapping generations, random mating, monoecious individuals, and no
101 selection. Two haplotypes sampled in the current population at time $t = 0$ have, as we go
102 backwards in time, a constant probability $(2N_c)^{-1}$ of coalescing at each generation, for the first t_c
103 generations, and then this probability switches to $(2N_0)^{-1}$ as we enter the ancestral
104 uncontracted population. We can approximate the distribution of coalescence time T of these
105 two haplotypes as a piecewise exponential distribution (see Appendix) with expected value:

$$106 \quad E[T] = 2(N_0 - N_c) e^{-t_c/2N_c} + 2N_c. \quad (1)$$

107 We see that the expected coalescence time decreases exponentially with the age of the
108 contraction t_c and that it approaches $2N_c$ for a very old contraction. Coalescence times cannot
109 be measured directly from empirical data, but they are closely related to nucleotide diversity π .
110 Under the infinitely many sites model, the number of nucleotide differences between two
111 homologous DNA segments is proportional to their coalescence time T as $\pi = 2\mu T$, where μ is
112 the total mutation rate for the whole segment. Multiplying eq. (1) by 2μ shows that an

113 instantaneous population contraction leads to an exponential decrease of the expected
 114 nucleotide diversity along the genome with the age of the contraction t_c . However, it does not
 115 inform us on the distribution of nucleotide diversity π along the genome, or on spatially
 116 correlated patterns of diversity such as local depletion or excess of diversity relative to the
 117 expectation.



118

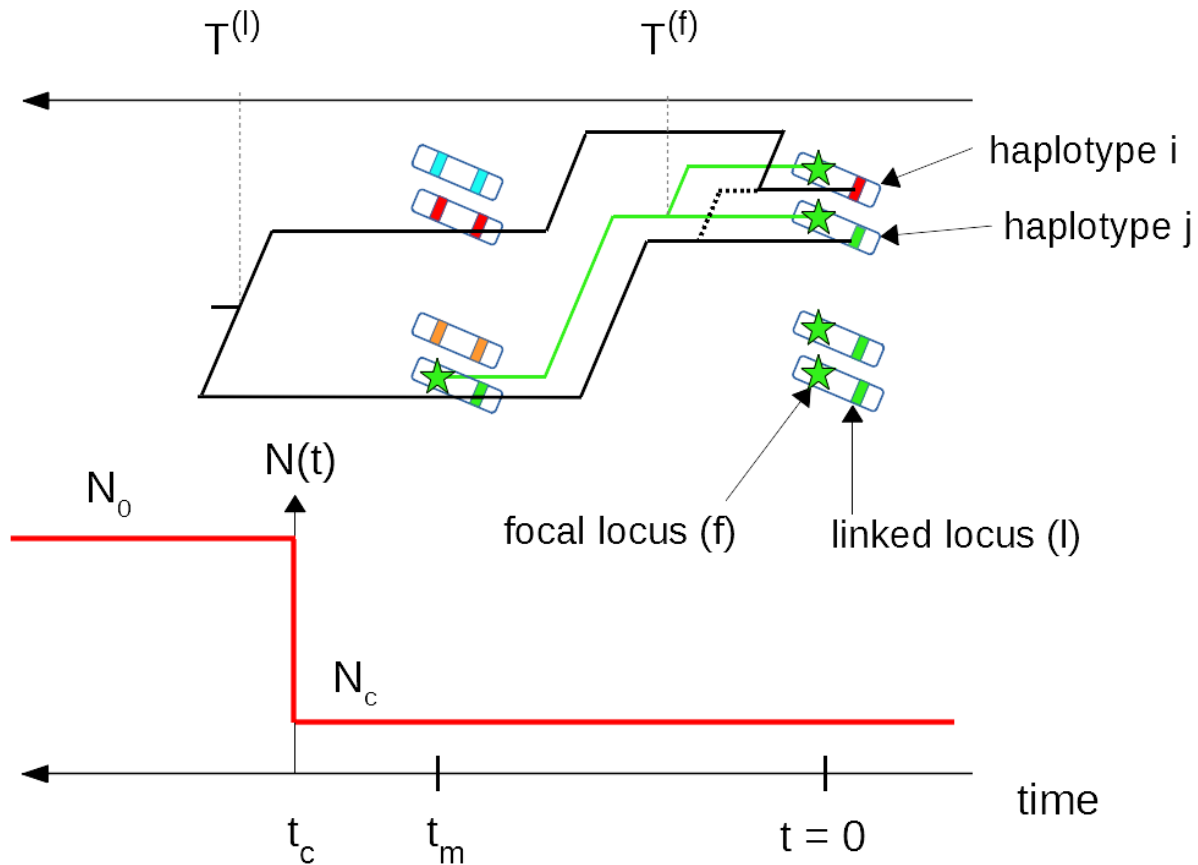
119 **Figure 1.** Nucleotide diversity of a population experiencing a contraction, as a function of the
 120 time t_c elapsed since the contraction, measured in units of $2N_c$. (a) distribution of nucleotide
 121 diversity as a function of time, nucleotide diversity along the chromosome at $t_c = 0$ (panel b), at
 122 $t_c = 0.25$ (panel c) and at $t_c = 0.75$ (panel d). Population size before contraction $N_0 = 2.37 \times 10^6$
 123 and after contraction $N_c = 4,400$. Mutation rate $\mu = 5.42 \times 10^{-10}$ per site per generation.
 124 Recombination rate $r = 3.5 \times 10^{-8}$ per site per generation. Chromosome size $L = 20$ Mb. Window
 125 size 10 Kb sliding at 1 Kb intervals. Sample size: 30 haplotypes. These parameters are taken from
 126 Rogers et al. (2010). Simulations were performed with fastsimcoal2 (Excoffier et al. 2021).

127

128 Fig. 1 shows the evolution of the distribution of π as a function of the time t_c elapsed since the
129 contraction. For $t_c = 0$, there is no contraction, and the population size remains constant and
130 equal to N_0 . In this case we see (fig. 1a,1b, $t_c = 0$) that the distribution of π is symmetric and
131 centered at $E[\pi] = 4N_0\mu$. For an older contraction, we see that the distribution is not only
132 shifted to lower values of diversity as expected from eq. (1), but that it also becomes strongly
133 peaked around $\pi = 4N_c\mu$. This bimodality of the distribution can be understood intuitively in the
134 following way. There are two possible types of coalescent trees for haplotypes sampled after
135 the population contraction (note that the tree depends on the locus considered because of
136 recombination). Indeed, the most recent common ancestor (MRCA) of the sample lived either
137 before the contraction ($T_{\text{MRCA}} > t_c$), or after the contraction ($T_{\text{MRCA}} < t_c$). In the former case, the
138 tree at this locus has long inner branches and short outer branches, whereas in the latter case,
139 the tree is essentially a (short) neutral tree corresponding to a population of constant size N_c
140 (Excoffier *et al.* 2009). Both types of trees occur at different loci and correspond to the two
141 observed modes in the distribution of the nucleotide diversity along the chromosome. The
142 precise shape of the distribution of nucleotide diversity across sites depends on the relative
143 frequency of both types of trees, which itself depends on the age of the contraction t_c . For a
144 sample of size two, the probability that the MRCA lived after the contraction, that is, $T_{\text{MRCA}} < t_c$
145 is $1 - e^{-t_c/2N_c}$. For a larger sample of haplotypes, there is no closed form solution for this
146 probability, but the trees rooted after the contraction are rare for $t_c \ll 2N_c$ and very frequent
147 when $t_c \gg 2N_c$ (Tavaré 1984). Therefore, the evolution of the distribution of π for increasing
148 contraction age t_c appears to be a transition from a unimodal distribution centered at $4N_0\mu$ to
149 another unimodal distribution centered at $4N_c\mu$, with both modes coexisting for intermediate
150 ages (fig. 1). This bimodality has been pointed out previously in the context of population
151 bottlenecks (Austerlitz *et al.* 1997); however, those studies mainly focused on long duration
152 bottlenecks (the effect of a contraction or a bottleneck on nucleotide diversity is the same
153 provided that the bottleneck is not yet finished, or that it finished very recently so that the
154 effect of population recovery is negligible). In the present work, we investigate the effect of
155 short contractions on the genetic diversity and make the claim that this short contraction
156 regime is of particular interest as it can lead, such as in fig. 1c, to genomic signatures similar to

157 those generated by positive selection acting on a few sites in an otherwise neutral genome.
158 More specifically, we want to quantitatively describe the reduction of diversity along the
159 genome that is observed around a locus with a small T_{MRCA} (such as in fig. 1c in the regions
160 around 10-11 and 19-20 Mb), where we observe a valley or trough of diversity. Akin to what is
161 done for selective sweeps, we consider the (neutral) fast fixation of an allele and analyze the
162 impact of hitchhiking on the genetic diversity of neighboring loci, and we refer to this process as
163 a neutral sweep.

164 To investigate neutral sweeps in our model, we consider the following scenario: t_m generations
165 ago a mutation occurred at a single site on the chromosome, which we call the focal site. We
166 further assume that this mutation has just fixed in the population, i.e., that it was segregating at
167 a frequency strictly lower than one in the last generation (at $t = 1$), and has now (at $t = 0$) a
168 frequency equal to one. We assume that the population contraction occurred t_c generations
169 ago, with $t_c \geq t_m$. As the mutant enters the population as a single allelic copy at the focal locus,
170 defined as a non-recombining region surrounding the focal site, this copy is a common ancestor
171 for all the copies ($2N_c$) present at fixation. However, it is not necessarily the most recent
172 common ancestor. Fig.2 shows a sketch of our model to help visualize how recombination can
173 maintain diversity at linked loci around a locus where a new mutation quickly fixed in the
174 population.



175

176 **Figure 2.** Instantaneous population contraction with a subsequent neutral fixation. A mutant
 177 (green star) appeared t_m generations ago and has just fixed neutrally in a diploid population
 178 that experienced a contraction t_c generations ago. We represent the population as a set of $2N_c$
 179 two-locus haplotypes that are painted so that the gene copies present at $t = 0$ can be traced
 180 back to $t = t_m$. Due to recombination, haplotype i carries a red gene copy at the linked locus at
 181 $t = 0$. Correspondingly, the coalescence time $T^{(l)}$ of the haplotypes i and j at the linked locus
 182 (black tree) is larger than t_m . On the other hand, the coalescence time $T^{(f)}$ at the focal locus
 183 (green tree) is smaller than t_m because at this locus all gene copies descend from the same
 184 haplotype (due to the fixation of the focal mutation).

185 Results

186 Average coalescence time at a linked locus

187 We can calculate the expected coalescence time $T^{(l)}$ of two randomly sampled haplotypes at a
 188 linked locus as a function of the recombination rate r from the focal locus. The idea is to
 189 consider two haplotypes with a given coalescence time $T^{(f)}$ at the focal locus, and then follow

190 the genealogy of the gene copies carried by these two haplotypes at the linked locus backward
191 in time, while considering possible recombination events. The expected coalescent time at the
192 linked locus is then

$$193 \quad E[T^{(l)}] = \left(1 - E\left[e^{-2r \sum_{t=1}^{T^{(f)}} (1 - \bar{x}_t)}\right]\right) (t_m + T_m) + E\left[T^{(f)} e^{-2r \sum_{t=1}^{T^{(f)}} (1 - \bar{x}_t)}\right] \quad (2)$$

194 where \bar{x}_t is the average frequency of the mutant (derived) allele at the focal locus at time t
195 counting backward from present. A detailed derivation of this equation is given in Appendix A4.
196 The first term of the right-hand side of eq. (2) corresponds to cases where lineages escape the
197 neutral sweep due to recombination, and still have not coalesced after t_m generations. In this
198 case we need to wait on average $T_m = 2(N_0 - N_c) e^{-(t_c - t_m)/2N_c} + 2N_c$ extra generations
199 before the lineages coalesce, due to the contraction that happened $t_c - t_m$ generations before
200 the focal mutation. The second term of the right-hand side of eq. (2) corresponds to cases
201 where the lineages cannot escape the sweep and are forced to coalesce at a time $T^{(l)} \leq t_m$.

202 **Distribution of coalescence times at the focal locus**

203 To evaluate eq. (2), we need to determine the probability distribution of the pairwise
204 coalescence times $T^{(f)}$ at the focal locus, as well as the expected frequency trajectory of the
205 derived allele. Even though this allele fixes neutrally in a population of constant size (the
206 contraction occurs prior to the mutation), the distribution of coalescent times at the focal locus
207 $T^{(f)}$ departs from the usual exponential distribution for a neutral coalescent process because the
208 allele fixes in exactly t_m generations, and hence the coalescence time for a randomly chosen
209 pair of haplotypes is at most t_m . Slatkin (1996) investigated the coalescent process within a
210 “mutant allelic class” that originated from a single mutation at a given time in the past. He
211 derived exact analytical results for the average pairwise coalescence time, but the coalescence
212 distribution itself can only be expressed with multidimensional integrals and obtaining a closed
213 form expression does not appear feasible. We therefore use a different approach: given a
214 particular fixation trajectory of the mutant allele, i.e. given the number of mutant copies N_μ at
215 each generation between $t = 0$ and $t = t_m$, we can express the coalescence time distribution
216 within the mutant allelic class, using the result of a coalescent in a population with a time-

217 dependent (but deterministic) size $N_\mu(t)$ (Griffiths and Tavaré 1994). Averaging over all
 218 possible trajectories of the mutation, we obtain:

$$219 \quad P(T^{(f)}) = \sum_{\{x_t\}} \left[\frac{1}{2N_c x_{T^{(f)}}} \prod_{t=1}^{T^{(f)}-1} \left(1 - \frac{1}{2N_c x_t} \right) \right] P(\{x_t\}) \quad (3a)$$

220 where $x_t = N_\mu(t)/(2N_c)$ is the frequency of the mutant t generations from fixation, and
 221 $P(\{x_t\})$ is the probability of a given trajectory. $P(\{x_t\})$ can be evaluated (see Appendix A2) and
 222 the sum in eq. (3a) can in principle be computed numerically; however, the number of
 223 trajectories to consider is prohibitive. As a first approximation, we can replace x_t by its
 224 expectation \bar{x}_t , i.e., we neglect the fluctuations of the trajectory around the mean to obtain

$$225 \quad P(T^{(f)}) \simeq \frac{1}{2N_c \bar{x}_{T^{(f)}}} \prod_{t=1}^{T^{(f)}-1} \left(1 - \frac{1}{2N_c \bar{x}_t} \right). \quad (3b)$$

226 The last step is to determine the average trajectory of an allele fixing in exactly t_m generations.
 227 Zhao *et al.* (2013) as well as Maruyama and Kimura (Maruyama and Kimura 1975) have
 228 investigated the characteristic trajectory of an allele fixing in a given time but they do not
 229 provide a closed form solution. Here, we use a different approach (also based on diffusion
 230 theory to obtain an approximation for the average trajectory of an allele fixing in exactly t_m
 231 generations, starting from a frequency p_0 . As detailed in the Appendix A2, we obtain

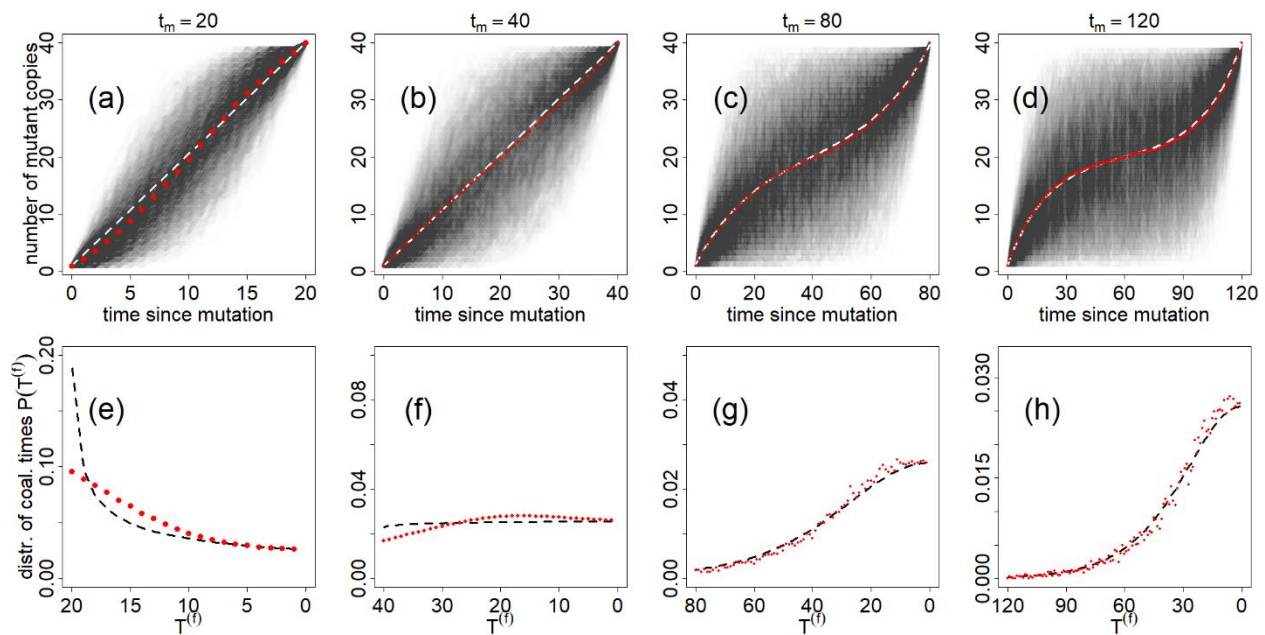
$$232 \quad \bar{x}_t = 1/2 \left(1 - (1 - 2p_0)e^{-(t_m-t)/N_c} + e^{-t/N_c} \right), \quad (4a)$$

233 which is valid for $t_m \gg 2N_c$. For very fast fixations, i.e., when $t_m \ll 2N_c$, the frequency of the
 234 allele increases approximately linearly as

$$235 \quad \bar{x}_t = 1 - (1 - p_0) \frac{t}{t_m}. \quad (4b)$$

236 We remind the reader that t is counted backwards from fixation. Fig. 3 compares equations (4a)
 237 and (4b) to trajectories obtained from simulations of a Wright-Fisher diploid population. We
 238 find good agreement between the simulations and the analytical results. Importantly, the
 239 typical neutral trajectory for large values of the fixation time has an “inverse-sigmoid shape”
 240 (fig. 3c), contrary to the typical sigmoid trajectory of a positively selected allele going to fixation
 241 in a constant size population (see fig. 5a). This neutral trajectory occurs because, conditional on

242 non-loss, neutral alleles need to quickly escape loss at the beginning and remain at
 243 intermediate frequencies to stay away from both fixation and loss until they eventually fix in
 244 the population at $t = 0$ (i.e. in exactly t_m generations). Fig. 3d-3f also shows the coalescence
 245 time distribution for several values of the fixation time t_m . The comparison of the distribution of
 246 pairwise coalescence time with numerical simulations of a Wright-Fisher model shows that our
 247 approximation eq. (3b) is quite accurate but overestimates the probability of coalescence for
 248 large coalescence times when t_m is small (fig. 3d). Notably, coalescence (simulated or
 249 theoretical) is more probable at large times (i.e. when the mutant appeared) for short fixation
 250 times (fig. 3d), whereas it is more probable at small times (i.e. close to fixation) for large
 251 fixation times (fig. 3e). The coalescence rate within the mutant allelic class is given by the
 252 inverse of the number of mutant copies and is for all values of the fixation time slightly more
 253 than $1/2N_c$ at the first generation. However, when the fixation time is short (fig. 3d), there is a
 254 fast increase of the coalescence rate backwards in time, and many lineages are forced to
 255 coalesce at $t = t_m$. When the fixation time is large (fig. 3f), the coalescence rate also increases
 256 backwards in time, but the increase is much slower. In that case, most coalescence events
 257 happen in much less than t_m generations, so that the early increase in frequency of the mutant
 258 has almost no influence on the coalescence distribution.



259

260 **Figure 3.** Average frequency (a-d) and coalescence time distribution (e-h) of an allele fixing in a
 261 diploid population of constant size $N_c = 20$ in exactly t_m generations, starting as a single copy

262 (i.e. $p_0 = (2N_c)^{-1}$). The red dots are the results of Wright-Fisher simulations, and the black and
263 white dashed lines are calculated with eqs. (4b) (first and second columns) (4a) (third and fourth
264 columns) and (3b). In panes (a-d) we show the variability of the fixation process by overlapping
265 1780 fixing trajectories. The (numerically estimated) probability, for a mutant that appears at
266 the onset of the contraction, to fix in less than t_m generations is 0.006, 0.16, 0.64 and 0.86 for
267 $t_m = 20, 40, 80$ and 120 respectively (for this particular value of N_c).

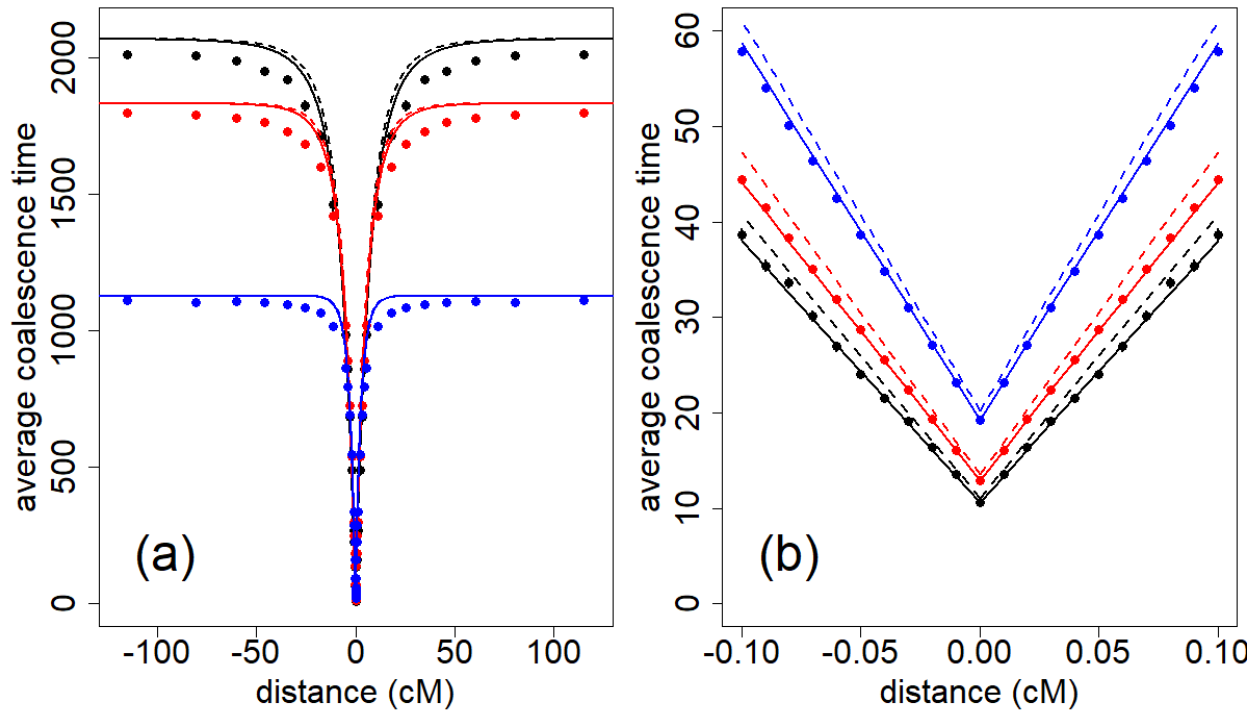
268 Effect of a neutral sweep on linked diversity

269 Combining equations (3b), (4a) with eq. (2) allows us to get an approximation for the average
270 coalescence time at linked loci. Since the derivation of eq. (2) assumes that there is at most one
271 recombination event in the genealogy of a randomly chosen pair of gene copies, we expect it to
272 be only accurate for small values of the recombination rate r . For large values of r we use a
273 heuristic approach combining the result of eq. (2), which is accurate for small r , and the
274 expected diversity at unlinked loci, which is equal to $T_0 = 2(N_0 - N_c) e^{-t_c/2N_c} + 2N_c$ as stated
275 in eq. (1). We fit the trough of diversity with an exponential function of the form:

$$276 \quad E[T^{(l)}](r) = T_0(1 - ce^{-ar}), \quad (5)$$

277 where the coefficients $c = 1 - E[T^{(f)}]/T_0$ and $a = 2E[(t_m + T_m - T^{(f)}) \sum_{t=1}^{T^{(f)}} (1 - \bar{x}_t)] / (T_0 -$
278 $E[T^{(f)}])$ are obtained by imposing that eqs. (2) and (5) coincide for small values of r (using a
279 linear expansion in r). On fig. 4 we compare the result of eq. (5) to Wright-Fisher simulations
280 with two recombining loci. We see in fig. 4a that the exponential function fits the data accurately
281 at large values of the recombination distance, but that the fit is biased for intermediate values of
282 r . In fig. 4b we see that the approximation is very good for low values of the recombination
283 distance, although there still is a slight bias. This discrepancy at small r can be corrected (solid
284 lines in fig. 4) if we use numerical estimations of \bar{x}_t and $P(T^{(f)})$, instead of eqs. (4) and (3b), to

285 evaluate eq. (5).



286

287 **Figure 4.** Average coalescence time at a linked locus, as a function of the recombination
 288 distance from the focal locus where a mutant fixed in exactly t_m generations, starting from a
 289 single copy t_m generations ago. $t_m = 15$ in black, $t_m = 20$ in red and $t_m = 40$ in blue. The dots are
 290 calculated with two-locus WF simulations, and compared to eq. (5) with either a numerical
 291 estimation (solid lines) or a theoretical estimation (dashed lines) of \bar{x}_t and $P(T^{(t)})$. $N_c = 20$. $N_0 =$
 292 1500. The population experienced a contraction $t_c = t_m$ generations ago.

293

294 We observe, as expected, on fig. 4 that the troughs of diversity induced by neutral sweeps are
 295 wider and deeper for short fixation times. Similarly to what happens after a selective sweep,
 296 there is less opportunity for linked loci to escape the sweep by recombination and maintain
 297 diversity when the fixation is fast. In addition, the diversity level at the center of the valley is
 298 given by the average coalescence time at the focal locus, which quickly decreases for small
 299 fixation times t_m .

300 Comparison of neutral sweeps and selective sweeps

301 Since we did not make any assumption regarding the process driving the mutant allele to
 302 fixation when deriving the average coalescence time at linked loci (eq. (2)) and the coalescence

303 time distribution at the focal locus (eq. (3b)), our framework allows us to directly compare the
304 signatures of different processes that can drive mutations to fixation in a given number of
305 generations. We illustrate this by comparing the effect of neutral and hard selective sweeps on
306 linked diversity. Later we will discuss how neutral sweeps compare to a larger variety of
307 scenarios (e.g. background selection, small selection coefficients, or dominant alleles). Here we
308 assume that the neutral and selected fixations occurred over the same time interval, that is in
309 both cases in exactly t_m generations. The selected fixation is assumed to be codominant ($h=0.5$)
310 and occurs on an autosomal locus in a randomly mating diploid population of constant size N_1 ,
311 and we consider a strong selection strength ($2N_1s \gg 1$) so that the allele frequency follows the
312 deterministic trajectory

$$313 \quad \bar{x}_t = \frac{1}{1 + (2N_1 - 1) e^{-2(1-t/t_m) \log(2N_1)}}, \quad (6)$$

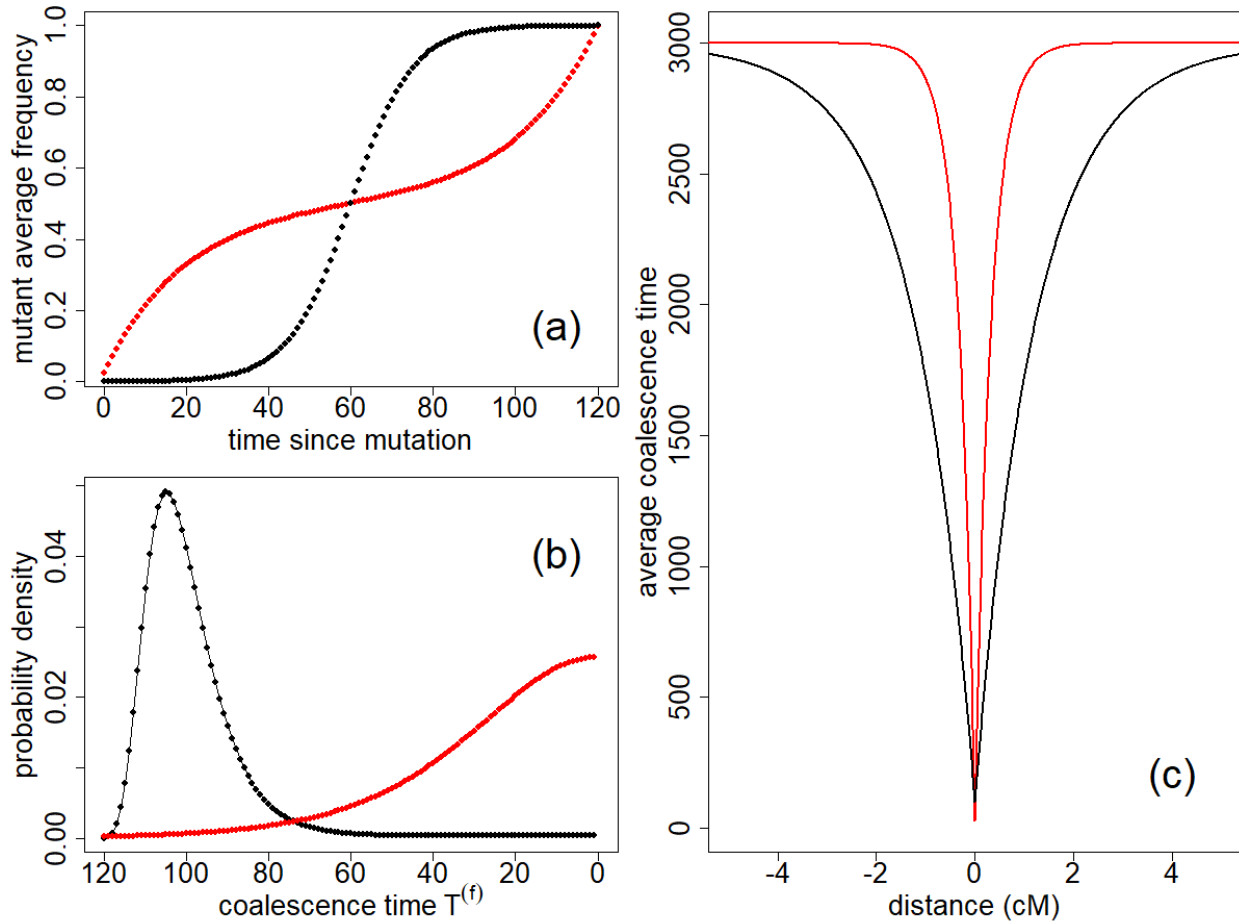
314
315 where the fixation time is given by $t_m(s) = 2\log(4N_1 s)/s$ (Barton 1995). Then combining eqs. (5),
316 (3b) and (6), we can compute the average coalescence time at linked loci as a function of the
317 recombination distance r to the focal locus, after replacing T_m , the average coalescence time at t
318 $= t_m$, by $2N_1$ in eq. (5) and N_c by N_1 in eq. (3b). This approach yields results similar to
319 Charlesworth (2020), where the author investigated signals of selective sweeps correcting for
320 coalescent events that happen during the sweep, thus going beyond the common assumption of a
321 star tree structure at the focal locus. For sake of simplicity in the neutral case, we consider that
322 the mutant appeared at the time of the contraction, i.e. $t_m = t_c$. Furthermore, we will assume that
323 the average coalescence times (and consequently the genetic diversity) are equal in both
324 scenarios, i.e. that $T_0 = 2N_1$ which implies that

325
$$N_0(t_m) = (N_1 - N_c) e^{t_m/2N_c} + N_c . \quad (7)$$

326 In the neutral case we want the diversity to remain as high as $4N_1\mu$ after the contraction, which

327 is possible only if the ancestral diversity was even higher, i.e. we have in general $N_0 > N_1 > N_c$.

328



329

330 **Figure 5.** Comparison between troughs of diversity resulting from a selective sweep (black) and

331 a neutral sweep (red), for the same fixation time $t_m = 120$ (corresponding to $s \approx 0.1$ in the

332 selective case). Frequency of the fixing allele as a function of time (a), coalescence time

333 distribution (b) and diversity around the fixing site along the genome using eq. (5) (c). $N_1 = 1500$,

334 $N_c = 20$ and $N_0 = 2.97 \times 10^4$.

335

336 In fig. 5a, we compare the mutant average frequency as a function of time for a selected and a

337 neutral fixation. The dynamics of the neutral fixation is the opposite of that of the selected

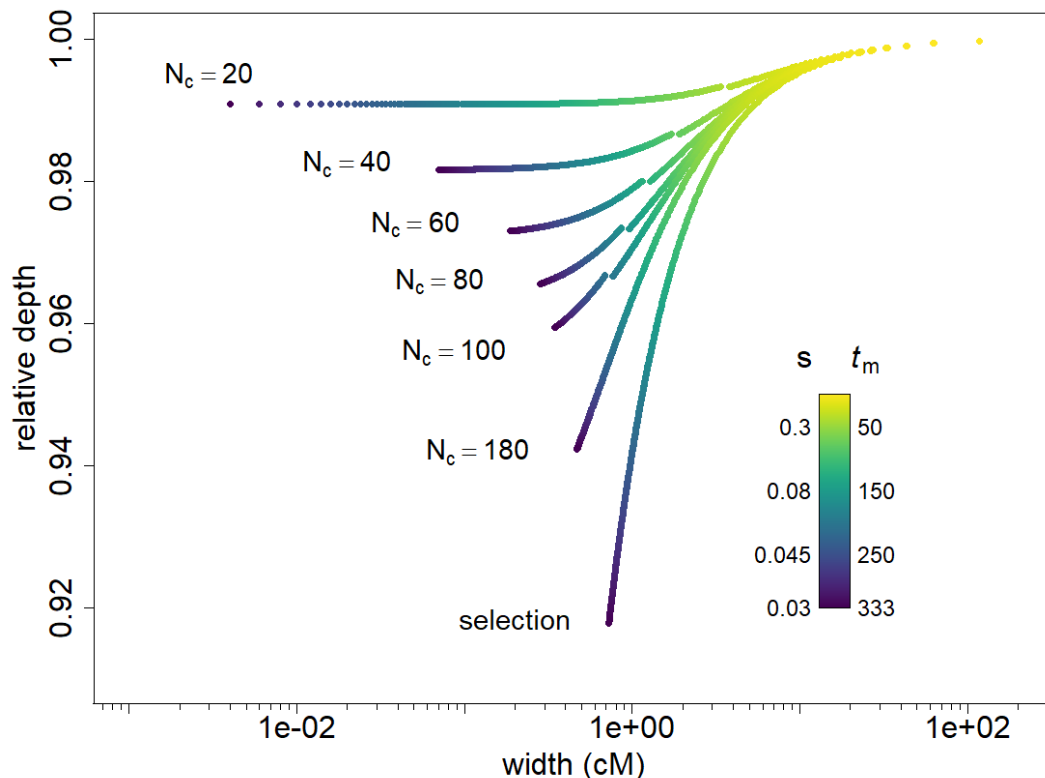
338 allele in the sense that when one is increasing, the other is “resting” and vice versa. These

339 different trajectories translate into different coalescence distributions at the focal locus (fig.

340 5b). If selection drives the fixation of the mutation, the distribution of coalescence time is
341 peaked at large coalescence times. In contrast, in the neutral case the distribution is skewed
342 towards small coalescence times. Correspondingly, the coalescence tree for the selected case
343 has a star-like structure (not shown), whereas the tree for the neutral case has shorter outer
344 branches. Therefore, for a given recombination distance, there will be fewer recombinations on
345 the neutral tree because it has a much smaller total length. As recombination helps maintain
346 diversity at linked loci, we would expect neutral troughs of diversity to be wider than in the
347 selected case. However, this is at odds with the valleys of diversity observed in fig. 5c, where
348 the selective trough is wider than the neutral trough. In fact, even though recombination is less
349 abundant on the neutral tree, it is more efficient at recovering diversity. Indeed, if at a linked
350 locus a pair of lineages escapes the sweep due to recombination, it takes on average an extra
351 $2N_1$ generations, counted backwards from generation $t = t_m$ when the mutant appeared, for
352 them to coalesce in the selective case, and an extra $2N_0$ generations in the neutral case. As $N_0 >$
353 N_1 two lineages escaping the sweep due to recombination have a larger coalescence time in the
354 neutral case, and correspondingly a larger diversity, which explains why the neutral valley of
355 diversity is narrower. Furthermore, we see that the trough is deeper in the neutral case (fig. 5c),
356 since the average coalescence time is smaller at the focal site due to the smaller total length of
357 the coalescence tree.

358
359 To determine if these differences between selective and neutral troughs hold for other fixation
360 times and population sizes, we define two quantities that characterize the shape of a trough, as
361 well as its propensity to be detected in real data: i) the trough relative depth and ii) the width of
362 the trough. The relative depth is defined as the difference between the background level of
363 diversity and the diversity at the focal locus, divided by the background diversity, and the width
364 is measured at half depth, i.e. halfway between the background diversity and the diversity at
365 the focal locus. On fig. 6 we plot the relative depth of neutral and selective troughs as a
366 function of their width for different fixation times t_m , calculated with our analytical expressions.
367 We see that the neutral troughs are not only always narrower than the selective troughs for the
368 same value of t_m , but also deeper. This is due to differences in the focal tree structure between

369 the selective case and the neutral case as well as difference in the ancestral background level in
370 both cases, as explained above. For very short fixation times (corresponding to selection
371 coefficients larger than 0.1), there is almost no difference between troughs generated by
372 selective and neutral sweeps. Indeed, for such values of t_m , in both cases the focal coalescence
373 tree is essentially a star tree because the increase in frequency is very fast, and the ancestral
374 backgrounds of diversity, $2N_0$ and $2N_1$, are also practically equal. Note however that at small t_m
375 the corresponding value of the selection coefficient s (see legend of fig. 6) may be
376 unrealistically high. For realistic values of the selection coefficient/fixation time, the neutral
377 troughs tend to be quite deep but narrow, whereas selective troughs are wider and their depth
378 decreases quickly for low selection coefficients. From fig. 6, we see that the shape of a neutral
379 trough is generally different from a selective sweep signal, but in practice those differences
380 might be hidden due to the noise inherent present in real genomic data, and it might be
381 difficult to decide whether a genomic signal is a due to a neutral sweep or a selective sweep.



382

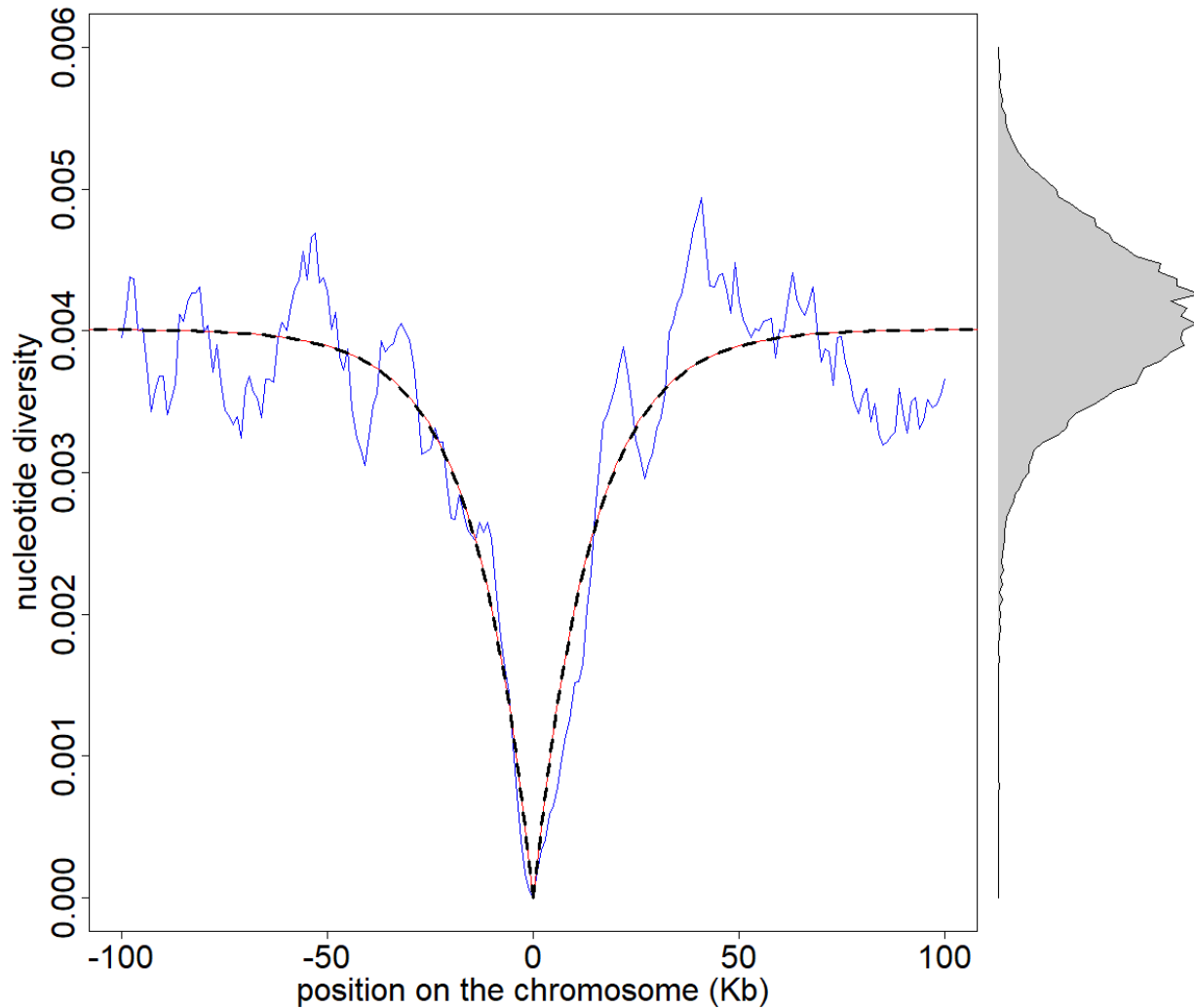
383 **Figure 6.** Relative depth as a function of the width of the diversity troughs, for different values
384 of t_m and N_c in the neutral case and for selective scenarios with identical fixation times. t_m goes
385 from 1 to 333 by increments of 1, the corresponding values of the selection coefficient s are

386 indicated on the left of the legend bar (for all of them we have $N_1 s \gg 1$). $N_1 = 1500$. N_0 is given
387 by eq. (7) and depends on N_c and t_m . The jumps in the neutral curves for $N_c = 20, 40, 60, 80$ and
388 100 are due to the use of two different approximations for the frequency of the mutant, eqs.
389 (4a) and (4b) and are located at $t_m = 2N_c$.

390 Is the Qtzl trough in *D. melanogaster* a neutral trough?

391 A region with reduced nucleotide diversity around the *Quetzalcoat1* gene identified in
392 *Drosophila melanogaster* was judged compatible with a selective sweep (Rogers *et al.* 2010). A
393 hard sweep model (Kaplan *et al.* 1989) was fitted assuming a constant population size of $N_1 =$
394 1.85×10^6 diploid individuals and it was inferred that a positively selected allele fixed in the
395 population 1.5×10^5 generations ago (1.5×10^4 years) due to a selective advantage of $s = 0.0098$
396 (corresponding to a fixation time of more than 300 years). Using our theory, we fitted the data
397 under a neutral demographic scenario of recent population size change that can generate
398 neutral troughs with the same width and almost the same relative depth (less than 0.1%
399 difference) as the *Quetzalcoat1* trough. To infer the demographic parameters, we measure the
400 width of the selective sweep curve used to fit the data in (Rogers *et al.* 2010) and find a set of
401 values of (N_c, t_m) that define a neutral trough with the same width. We then impose that $t_m/2N_c$
402 $= 0.25$ so that the troughs are rare yet observable along the chromosome as explained on fig. 1,
403 and we obtain $t_m = 2200$ and $N_c = 4400$. In fig. 7 we show a trough generated during a
404 population contraction corresponding to these inferred values, using the software fastsimcoal2
405 (Excoffier *et al.* 2021). We see that the neutral sweep fit is almost indistinguishable from the
406 selective sweep fit because they not only have the same width, but also practically the same
407 depth. Note that this simulated trough can be also seen in fig. 1c in the region 19-20 Mb. The
408 same approach can be used to generate neutral troughs with a broad range of width and depth,
409 which implies that in most cases, an alternative demographic neutral scenario can be
410 compatible with a trough that is putatively due to selection. In practice, model inference does
411 not rely solely on the fitting of a single trough, and genome wide information must be used.
412 Therefore, we do not exclude here the possibility of the presence of adaptation in the
413 *Quetzalcoat1* gene, but rather make the general warning that valleys of diversity do not
414 necessarily indicate the presence of positive selection.

415 The authors affirm that all data necessary for confirming the conclusions of the article are
416 present within the article, figures, and tables.



417

418 **Figure 7.** Trough of nucleotide diversity observed on a 20 Mb chromosome simulated with
419 *fastsimcoal2*. The population experienced a contraction 2200 generations ago and the (diploid)
420 population size was reduced from $N_0 = 2.37 \times 10^6$ to $N_c = 4400$. The nucleotide diversity (blue line)
421 is calculated on a sample of 30 haplotypes from our simulation. The black dashed line is the
422 expected diversity (eq. (5)) for an allele that just fixed neutrally in the population, starting as a
423 single copy 2200 generations ago. The red line is the expectation of a hard selective sweep with
424 selection coefficient $s = 0.0098$. On the right we plot the distribution of nucleotide diversity for
425 the whole chromosome. The mutation rate $\mu = 5.42 \times 10^{-10}$ per site per generation, and
426 recombination rate $r = 3.5 \times 10^{-8}$ per site per generation were taken from (Rogers et al. 2010).
427 The nucleotide diversity (in blue) is calculated for sliding windows of 10 Kb at 1 Kb intervals.

428 Discussion

429 It has repeatedly been suggested that strong depletions of diversity in the genome are not
430 necessarily due to the presence of positive selection (Johri *et al.* 2020), and can also be the
431 result of demographic effects only, such as the allele surfing phenomenon occurring at the front
432 of a range expansion (Klopfstein *et al.* 2006). In this work, we considered a model of population
433 contraction to analyze quantitatively the genomic signature of the rapid fixation of a mutation
434 during a population contraction. Taking a step further from previous work that focused on the
435 impact of range expansion on mere allele frequencies, we have studied here the impact of a
436 neutral allele fixation on neighboring genomic diversity. We show that the diversity profile
437 around a recently fixed locus crucially depends on the frequency trajectories of the allele going
438 to fixation, and we outline the fact that neutrally fixing alleles have an inverse-sigmoid
439 trajectory (fig. 3c), as compared to the standard sigmoid frequencies observed for positively
440 selected alleles. For the same fixation time, this difference translates into different genomic
441 signatures (see figs. 5c and 6). Our results demonstrate that there is a short period after a
442 demographic contraction (or during a range expansion) where observed profiles of genomic
443 diversity would look like those usually attributed to selection (fig. 1c), and that selective sweep
444 signals can be mimicked by neutrally fixing mutations without the need to invoke complex
445 histories of population size changes.

446 Our results allow for a systematic comparison of selective and neutral troughs of diversity, and
447 we used our results to investigate trough shapes for range of neutral and selected scenarios
448 (see fig. 6), which in principle can be used to decide whether a given empirical trough is due to
449 selection or demography, and to infer the corresponding parameters. However, we did not
450 consider the whole spectrum of possible selection scenarios. It would be indeed interesting to
451 use our results to study cases of background selection, small selection coefficients, and a
452 variety of dominance coefficients. All these cases should have their own characteristic
453 trajectories of fixation, and hence potentially different genomic signatures. In addition, in our
454 model we do not consider mutations that fixed in the past (we always assume that the allele
455 has just reached fixation), nor do we consider mutations appearing before the population
456 contraction, i.e., with $t_m > t_c$. The average coalescence time in the former case can be expressed

457 as a function of the coalescence time at fixation using conditional probabilities, and we can
458 show that a sweep signal vanishes exponentially with the time elapsed since fixation (see
459 Appendix A4). In the latter case, we can solve the problem by considering the number of gene
460 copies at t_c that descend from the original copy that appeared at t_m . One could extend our
461 results by considering an allele starting from an arbitrary number of copies at t_c , akin to soft
462 selective sweeps; however, the analytic calculations are complex, and we leave this study for
463 future research. In any case, those additional scenarios must be considered when trying to infer
464 models from the study of troughs found in empirical data. Another phenomenon that renders
465 the inference of parameters cumbersome is a possible interference between troughs. Indeed,
466 when two loci fix neutrally in the population, the genetic diversity in the region between those
467 loci will be influenced by both fixations and will differ from the diversity expected in the vicinity
468 of a single fixing locus. As in the case of interference between the fixation of selected alleles
469 (Weissman and Barton 2012), this should limit the number of independent neutral fixations.
470 The effect of trough interference is stronger for neighboring troughs, and the probability to
471 observe close troughs depends on the relative frequency of troughs along the genome, which
472 itself depends on the distribution of the T_{MRCA} . In fig. 1d for example, the distribution of T_{MRCA}
473 has a mode centered around $4N_c$ (not shown) and correspondingly the nucleotide diversity is
474 peaked around $4N_c \mu$. As a result, we see many regions of the chromosome with a low diversity.
475 It is likely that those troughs interfere with each other and that they do not correspond to the
476 profile of an isolated trough. On the other hand, in fig. 1c, the first mode of the T_{MRCA}
477 distribution is truncated because t_c is much smaller than $4N_c$, and only T_{MRCA} s equal or close to
478 t_c are observed (plus all the T_{MRCA} s corresponding to the second mode centered at $4N_0$). In this
479 case there is no interference and the (rare) troughs, such as the one in fig. 7, are correctly fitted
480 by their theoretical expectation. Those considerations imply that, even though we know the
481 forward in time probability that an allele will fix in t_m generations, it is difficult to infer the
482 parameters of a fixation scenario from a single observed neutral valley of diversity. It appears
483 therefore difficult to perform model selection from a single trough signal, i.e., to decide
484 whether a particular trough is due to selection or demographic effects, because alternative
485 demographic scenarios that we did not consider here could also lead to similar signals. In

486 principle, if several troughs of diversity were observed in a genome, one could use the
487 distribution of trough shapes expected under a given simple demographic model and a
488 distribution of fitness effect to compare neutral and selection models under a likelihood
489 framework.

490 In conclusion, our results suggest that any empirical valley of diversity found in empirical data
491 can be reproduced neutrally with a population contraction using appropriate parameters. One
492 could argue that this identifiability problem disappears once the true evolutionary history is
493 correctly inferred. However, inferring the true demographic history requires precise knowledge
494 about how selection has shaped genomic diversity (Johri *et al.* 2020). In humans, for instance, it
495 has been estimated that roughly 95 % of genomic diversity is affected by some form of non-
496 neutral forces such as background selection or biased gene conversion (Pouyet *et al.* 2018)
497 potentially biasing demographic inference (Ewing and Jensen 2016). These considerations
498 indicate that genome scans in search for signals of adaptation might be subject to stronger
499 false positive rates than previously thought. We thus believe that despite current advances
500 using supervised machine learning or similar approaches (Schridder and Kern 2018), it remains
501 important to further study the effect of neutral fixations in various demographic scenarios using
502 localized genomic approaches such as the present analytical work (Johri *et al.* 2021b); as well as
503 with controlled experiments on real living organisms where both the selected locus and the
504 population history are known (Orozco-terWengel *et al.* 2012). Such work will be critical in order
505 to develop more appropriate evolutionary null models for statistical inference (Hahn 2008;
506 Johri *et al.* 2020).

507 Appendix

508 A1. Coalescence distribution after a contraction

509 We want to determine the coalescence time of two lineages in a population that experienced a
510 contraction t_m generations ago, from a diploid size N_0 to N_c . As we go backward in time, the
511 coalescence rate switches from $(2N_c)^{-1}$ to $(2N_0)^{-1}$ at $T = t_c$. The probability distribution might
512 still be approximated by a piecewise exponential density:

$$\begin{aligned}
 f_0(T) &= \frac{1}{2N_c} \exp\left(-\frac{T}{2N_c}\right) \text{ for } 0 < T < t_c \\
 &= \frac{1}{2N_0} \exp\left(-\frac{t_c}{2N_c}\right) \exp\left(-\frac{T-t_c}{2N_0}\right) \text{ for } T \geq t_c
 \end{aligned}$$

The corresponding expectation for this distribution is

$$\begin{aligned}
 E[T] = T_0 &= \int_0^{\infty} T f_0(T) dT \\
 &= 2N_0 e^{-t_c/2N_c} + 2N_c(1 - e^{-t_c/2N_c})
 \end{aligned}$$

A2. Average frequency of an allele fixing in exactly t_m generations

In this section time is counted forward from the mutation, which appears after the contraction, so that during the fixation the diploid population size is constant and equal to N_c . We condition on the fixation time t_m of the mutant. We define the trajectory of a mutant as the list of frequencies at all generations: $\{x_t\} = (x_0, x_1, \dots, x_{t_m-1}, x_{t_m})$. We assume that the mutant fixes in exactly t_m generations, starting from a frequency p_0 , i.e. $x_0 = p_0$, $0 < x_{t_m-1} < 1$ and $x_{t_m} = 1$. The probability that the mutant follows a given trajectory might be expressed as the product of the transition probabilities

$$P(\{x_t\}) = \prod_{t=0}^{t_m-1} P(i, t \rightarrow j, t+1 \mid \text{fix in } t_m, p_0)$$

For an unconditional Wright Fisher model, $P(i, t \rightarrow j, t+1)$ is the probability to have j copies of the new allele at $t+1$ given that there were i copies at t . We note $P_t(i \rightarrow j)$ for brevity. If we only consider trajectories fixing in exactly t_m generations and starting from a number $2N_c p_0$ of copies at $t=0$, then the transition probabilities are not equal to the transitions of the unconditional Wright-Fisher model. However, thanks to Bayes theorem, we can write

$$\begin{aligned}
 P_t(i \rightarrow j \mid \text{fix in } t_m, p_0) &= \frac{P_t(\text{fix in } t_m \mid i \rightarrow j, p_0) P_t(i \rightarrow j \mid p_0)}{P(\text{fix in } t_m \mid p_0)} \\
 &= \frac{P(\text{fix in } t_m \mid j_{t+1}) P_t(i \rightarrow j)}{P(\text{fix in } t_m \mid p_0)} \quad (S1)
 \end{aligned}$$

531 From the first to the second line, we use the Markov property. The three terms involved in the
 532 right-hand side of this equation can be approximated thanks to diffusion theory. In this
 533 framework, the probability for an allele to fix in t_m generations, given that there were i copies
 534 at time t is approximately (Ewens 2004, taking the time derivative of eq. 5.39)

$$535 \quad P(\text{fix in } t_m | i_t) = \frac{3}{2N_c} \left(1 - \frac{i}{2N_c}\right) \frac{i}{2N_c} e^{-(t_m-t)/2N_c}$$

536 The term $P_t(i \rightarrow j)$ is the unconditional binomial transition probability of the Wright Fisher
 537 model (which does not depend on t). In principle, eq. (S1) can be used to compute the exact
 538 distribution of coalescence times at the focal locus, using eq. (3a). However, the huge number
 539 of possible trajectories fixing in t_m generations ($(2N_c - 1)^{t_m-1}$) makes the average over
 540 trajectories impossible to evaluate numerically. For this reason, we use the approximation in
 541 eq. (3b).

542 We consider here the probability that the allele has frequency x at time t , given that it started
 543 at frequency p_0 at $t = 0$. Again if we only consider trajectories that fix in exactly t_m
 544 generations, this probability is not equal to the neutral diffusive result. However, similarly to
 545 the previous section, we can use Bayes theorem:

$$546 \quad P(x_t | \text{fix in } t_m, p_0) = \frac{P(\text{fix in } t_m | x_t)P(x_t | p_0)}{P(\text{fix in } t_m | p_0)}$$

547 From diffusion theory (Ewens 2004, eq. 5.11), we also have

$$548 \quad P(x_t | p_0) = 6p_0(1 - p_0) e^{-t/2N_c} (1 + 5(1 - 2p_0)(1 - 2x)e^{-t/N_c})$$

549 which is a second order expansion of an infinite series involving vanishing exponential terms
 550 ($e^{-k(k+1)t/4N_c}$ for all $k \geq 1$). This expansion is thus valid in the limit of large times $t \gg 2N_c$. We
 551 deduce that the probability that an allele fixing in t_m generations has frequency x at time t is

$$552 \quad P(x_t | \text{fix in } t_m, p_0) = 6x(1 - x) (1 + 5(1 - 2p_0)(1 - 2x)e^{-t/N_c})$$

$$553 \quad \text{which yields } E[x_t | \text{fix in } t_m, p_0] = 1/2(1 - (1 - 2p_0)e^{-t/N_c})$$

554 This expression is valid for $t_m \gg t \gg 2N_c$, and does not allow to estimate the frequency close
555 to fixation (we see that $E[x_t]$ tends to $1/2$ as time grows). However, invoking a symmetry
556 argument we may write

$$557 \quad E[x_t | \text{fix in } t_m, p_0] = 1/2(1 - (1 - 2p_0)e^{-t/N_c} + e^{-(t_m-t)/N_c})$$

558 When $t_m \ll 2N_c$, we can use a linear approximation for the trajectory (based on the numerical
559 observations)

$$560 \quad E[x_t | \text{fix in } t_m, p_0] = p_0 + (1 - p_0) \frac{t}{t_m}$$

561 **A3. Coalescence distribution at linked loci around a neutral fixation**

562 We now return to the scenario of fig. 2, with a backward in time approach. Using Bayes
563 theorem, we express the coalescence time of two haplotypes at the linked locus $T^{(l)}$,
564 conditioning on the coalescence time at the focal locus $T^{(f)}$

$$565 \quad P(T^{(l)}) = \int_0^{t_m} P(T^{(l)} | T^{(f)}) P(T^{(f)}) dT^{(f)} = E[P(T^{(l)} | T^{(f)})]$$

566 We assume that the linked locus is close to the focal locus on the chromosome, more precisely
567 that the recombination rate r is very small $r \ll 1$, so that we consider at most one
568 recombination, occurring on one of the two focal lineages. We distinguish cases where there is
569 no recombination between $t = 0$ and $t = T^{(f)}$, cases where the allele at the linked locus
570 recombines (somewhere between $t = 0$ and $t = T^{(f)}$) onto a haplotype carrying the ancestral
571 allele at the focal locus, and cases where the allele at the linked locus recombines onto a
572 haplotype carrying the derived allele at the focal locus. We call the second and third case
573 homozygous and heterozygous recombination respectively, referring to the zygosity at the focal
574 locus of the recombining pair of haplotypes (note that are three haplotypes, the two first ones
575 have a coalescence time $T^{(f)}$, and the third one recombines with one of these two). If there is no
576 recombination, then the coalescence time is the same for both loci, $T^{(l)} = T^{(f)}$. To treat the case
577 with a homozygous recombination, it is convenient to name the haplotypes: i and j coalesce at
578 $T_{ij}^{(f)} = T^{(f)}$ at the focal locus, and k is a third haplotype, onto which the linked allele recombines

579 (coming from i). The linked allele carried by j stays on the same haplotype (no more than one
 580 recombination), and after recombining onto k , the linked allele initially carried by i also stays on
 581 k (again, at most one recombination). This implies that those two linked alleles coalesce at $T_{ij}^{(l)} =$
 582 $T_{jk}^{(f)}$. This time is in general different than $T_{ij}^{(f)}$, however on average $T_{jk}^{(f)}$ and $T_{ij}^{(f)}$ are equal
 583 (averaging over all possible coalescence trees at the focal locus). This implies that we can treat
 584 the case with homozygous recombination as if there was no recombination. If there is a
 585 heterozygous recombination between i and k , at some generation between $t = 0$ and $t = T^{(f)}$,
 586 then the linked alleles still have not coalesced at $t = t_m$ because after the recombination one of
 587 them is linked to a derived focal allele and the other one to an ancestral focal allele (and they
 588 stay linked because there is at most one recombination). In that case, $T_{ij}^{(l)}$ is equal to t_m plus a
 589 random time given by (on average) T_m , and is independent of $T_{ij}^{(f)}$. Using again Bayes theorem
 590 and the previous results to write

$$\begin{aligned}
 591 \quad P(T^{(l)} | T^{(f)}) &= P(T^{(l)} | T^{(f)}, \text{ one het. rec. in } [0, T^{(f)}])P(\text{one het. rec. in } [0, T^{(f)}]) \\
 592 &\quad + P(T^{(l)} | T^{(f)}, \text{ no het. rec. in } [0, T^{(f)}])P(\text{no het. rec. in } [0, T^{(f)}]) \\
 593 &= f_m(T^{(l)} - t_m)[1 - P(\text{no het. rec. in } [0, T^{(f)}])] \\
 594 &\quad + \delta(T^{(l)} - T^{(f)})P(\text{no het. rec. in } [0, T^{(f)}])
 \end{aligned}$$

595 Where $\delta(\cdot)$ is the Dirac delta function, and f_m is the unconditional coalescence distribution of a
 596 pair of lineages sampled at $t = t_m$, i.e. it is equal to the function f_0 introduced above but
 597 replacing t_c by $t_c - t_m$ (note also that $f_m(t) = 0$ if $t < 0$). We then have to evaluate the
 598 probability that there is no heterozygous recombination. At generation t (counted backward)
 599 the probability that a linked allele recombines onto a haplotype carrying the ancestral allele at
 600 the focal locus is $r(1 - x_t)$, where x_t is the frequency of the derived allele at the focal locus,
 601 we deduce that the probability that there is no heterozygous recombination on either lineage is

$$\begin{aligned}
 602 \quad P(\text{no het. rec. in } [0, T^{(f)}]) &= \prod_{t=1}^{T^{(f)}} (1 - r[1 - x_t])^2 \\
 &\simeq \exp\left(-2r \sum_{t=1}^{T^{(f)}} (1 - x_t)\right)
 \end{aligned}$$

603 This probability depends explicitly on the allele trajectory, which means that rigorously, all the
 604 calculations should be conditioned on a given trajectory, and then averaged over all
 605 trajectories. To allow for mathematical tractability, and to avoid heavy expressions, we consider
 606 that as a good approximation $x_t = \bar{x}_t$. Finally we obtain

$$\begin{aligned}
 607 \quad P(T^{(l)}) = & E \left[\delta(T^{(l)} - T^{(f)}) \exp \left(-2r \sum_{t=1}^{T^{(f)}} (1 - x_t) \right) \right] \\
 608 \quad & + f_m(T^{(l)} - t_m) E \left[1 - \exp \left(-2r \sum_{t=1}^{T^{(f)}} (1 - x_t) \right) \right]
 \end{aligned}$$

609 The expectation corresponding to this distribution yields eq. (2).

610

611 **A4. Average coalescence time at a linked locus around a mutation that completed fixation t_{fix}**
 612 **generations ago**

613 Thanks to Bayes theorem we can write

$$614 \quad E[T^{(l)}] = E[T^{(l)} | T^{(l)} < t_{\text{fix}}] P(T^{(l)} < t_{\text{fix}}) + E[T^{(l)} | T^{(l)} > t_{\text{fix}}] P(T^{(l)} > t_{\text{fix}})$$

615 i.e. we distinguish coalescence events happening in less than t_{fix} generations or more than t_{fix}

616 generations. In the former case, the coalescence is neutral, unconditional (the fixation is

617 completed) and happens in a population of constant size N_c which means that

618 $E[T^{(l)} | T^{(l)} < t_{\text{fix}}]$ and $P(T^{(l)} < t_{\text{fix}})$ can be worked out from the neutral exponential

619 distribution. On the other hand, $E[T^{(l)} | T^{(l)} > t_{\text{fix}}]$ is equal to t_{fix} plus the expectation from eq.

620 (5) which we note here $E[T^{(l)}](t = t_{\text{fix}})$. We obtain

$$621 \quad E[T^{(l)}] = 2N_c(1 - e^{-t_{\text{fix}}/2N_c}) + E[T^{(l)}](t = t_{\text{fix}}) e^{-t_{\text{fix}}/2N_c}$$

622 We see that the sweep signal vanishes exponentially with the time elapsed since fixation.

623 Acknowledgment

624 This work was partially supported by a Swiss NSF grant No 310030_188883 to LE. We are
625 grateful to Montgomery Slatkin, Brian Charlesworth and Jeff Jensen for their helpful comments.

626 Bibliography

627

628 Andolfatto P., and M. Przeworski, 2000 A genome-wide departure from the standard neutral
629 model in natural populations of *Drosophila*. *Genetics* 156: 257–268.

630 Austerlitz F., B. Jung-Muller, B. Godelle, and P.-H. Gouyon, 1997 Evolution of coalescence
631 times, genetic diversity and structure during colonization. *Theor. Popul. Biol.* 51: 148–
632 164.

633 Barton N. H., 1995 Linkage and the limits to natural selection. *Genetics* 140: 821–841.

634 Charlesworth B., M. T. Morgan, and D. Charlesworth, 1993 The effect of deleterious mutations
635 on neutral molecular variation. *Genetics* 134: 1289–1303.

636 Charlesworth D., B. Charlesworth, and M. T. Morgan, 1995 The pattern of neutral molecular
637 variation under the background selection model. *Genetics* 141: 1619–1632.

638 Charlesworth B., 2013 Background selection 20 years on: the Wilhelmine E. Key 2012
639 invitational lecture. *J. Hered.* 104: 161–171.

640 Charlesworth B., 2020 How Good Are Predictions of the Effects of Selective Sweeps on Levels
641 of Neutral Diversity? *Genetics* 216: 1217–1238.

- 642 Corbett-Detig R. B., D. L. Hartl, and T. B. Sackton, 2015 Natural selection constrains neutral
643 diversity across a wide range of species. *PLoS Biol.* 13: e1002112.
- 644 Crisci J. L., Y.-P. Poh, S. Mahajan, and J. D. Jensen, 2013 The impact of equilibrium
645 assumptions on tests of selection. *Front. Genet.* 4: 235.
- 646 Edmonds C. A., A. S. Lillie, and L. Luca Cavalli-Sforza, 2004 Mutations arising in the wave
647 front of an expanding population. *Proc. Natl. Acad. Sci. U. S. A.* 101: 975–979.
- 648 Ewens W. J., 2004 *Mathematical Population Genetics: I. Theoretical Introduction*. Springer,
649 New York, NY.
- 650 Ewing G. B., and J. D. Jensen, 2016 The consequences of not accounting for background
651 selection in demographic inference. *Mol. Ecol.* 25: 135–141.
- 652 Excoffier L., N. Marchi, D. A. Marques, R. Matthey-Doret, A. Gouy, *et al.*, 2021 fastsimcoal2:
653 demographic inference under complex evolutionary scenarios. *Bioinformatics*.
654 <https://doi.org/10.1093/bioinformatics/btab468>
- 655 Excoffier L., M. Foll, and R. J. Petit, 2009 Genetic Consequences of Range Expansions. *Annu.*
656 *Rev. Ecol. Evol. Syst.* 40: 481–501.
- 657 Galtier N., and M. Rousselle, 2020 How Much Does Ne Vary Among Species? *Genetics* 216:
658 559–572.
- 659 Griffiths R. C., and S. Tavaré, 1994 Ancestral inference in population genetics. *Stat. Sci.* 9: 307–
660 319.
- 661 Hahn M. W., 2008 Toward a selection theory of molecular evolution. *Evolution* 62: 255–265.

- 662 Hallatschek O., and D. R. Nelson, 2008 Gene surfing in expanding populations. *Theor. Popul.*
663 *Biol.* 73: 158–170.
- 664 Jensen J. D., Y. Kim, V. B. DuMont, C. F. Aquadro, and C. D. Bustamante, 2005 Distinguishing
665 between selective sweeps and demography using DNA polymorphism data. *Genetics*
666 170: 1401–1410.
- 667 Jensen J. D., B. A. Payseur, W. Stephan, C. F. Aquadro, M. Lynch, *et al.*, 2019 The importance
668 of the Neutral Theory in 1968 and 50 years on: A response to Kern and Hahn 2018.
669 *Evolution* 73: 111–114.
- 670 Johri P., B. Charlesworth, and J. D. Jensen, 2020 Toward an Evolutionarily Appropriate Null
671 Model: Jointly Inferring Demography and Purifying Selection. *Genetics* 215: 173–192.
- 672 Johri P., B. Charlesworth, E. K. Howell, M. Lynch, and J. D. Jensen, 2021a Revisiting the
673 Notion of Deleterious Sweeps. *Genetics*. <https://doi.org/10.1093/genetics/iyab094>
- 674 Johri P., K. Riall, H. Becher, L. Excoffier, B. Charlesworth, *et al.*, 2021b The Impact of
675 Purifying and Background Selection on the Inference of Population History: Problems
676 and Prospects. *Mol. Biol. Evol.* 38: 2986–3003.
- 677 Kaiser V. B., and B. Charlesworth, 2009 The effects of deleterious mutations on evolution in
678 non-recombining genomes. *Trends Genet.* 25: 9–12.
- 679 Kaplan N. L., R. R. Hudson, and C. H. Langley, 1989 The “hitchhiking effect” revisited.
680 *Genetics* 123: 887–899.
- 681 Kingman J. F. C., 1982a The coalescent. *Stochastic Process. Appl.* 13: 235–248.

- 682 Kingman J. F. C., 1982b On the genealogy of large populations. *J. Appl. Probab.* 19A: 27–43.
- 683 Klopstein S., M. Currat, and L. Excoffier, 2006 The fate of mutations surfing on the wave of a
684 range expansion. *Mol. Biol. Evol.* 23: 482–490.
- 685 Maruyama T., and M. Kimura, 1975 Moments for sum of an arbitrary function of gene frequency
686 along a stochastic path of gene frequency change. *Proc. Natl. Acad. Sci. U. S. A.* 72:
687 1602–1604.
- 688 Mathew L. A., and J. D. Jensen, 2015 Evaluating the ability of the pairwise joint site frequency
689 spectrum to co-estimate selection and demography. *Front. Genet.* 6: 268.
- 690 Maynard Smith J., and J. Haigh, 1974 The hitch-hiking effect of a favorable gene. *Genet. Res.*
691 23: 23–35.
- 692 Nicolaisen L. E., and M. M. Desai, 2013 Distortions in genealogies due to purifying selection
693 and recombination. *Genetics* 195: 221–230.
- 694 O’Fallon B. D., J. Seger, and F. R. Adler, 2010 A continuous-state coalescent and the impact of
695 weak selection on the structure of gene genealogies. *Mol. Biol. Evol.* 27: 1162–1172.
- 696 Orozco-terWengel P., M. Kapun, V. Nolte, R. Kofler, T. Flatt, *et al.*, 2012 Adaptation of
697 *Drosophila* to a novel laboratory environment reveals temporally heterogeneous
698 trajectories of selected alleles. *Mol. Ecol.* 21: 4931–4941.
- 699 Peischl S., I. Dupanloup, M. Kirkpatrick, and L. Excoffier, 2013 On the accumulation of
700 deleterious mutations during range expansions. *Mol. Ecol.* 22: 5972–5982.

- 701 Peischl S., and L. Excoffier, 2015 Expansion load: recessive mutations and the role of standing
702 genetic variation. *Mol. Ecol.* 24: 2084–2094.
- 703 Pouyet F., S. Aeschbacher, A. Thiéry, and L. Excoffier, 2018 Background selection and biased
704 gene conversion affect more than 95% of the human genome and bias demographic
705 inferences. *Elife* 7: e36317.
- 706 Pouyet F., and K. J. Gilbert, 2019 Towards an improved understanding of molecular evolution:
707 the relative roles of selection, drift, and everything in between. *arXiv [q-bio.PE]*.
- 708 Rogers R. L., T. Bedford, A. M. Lyons, and D. L. Hartl, 2010 Adaptive impact of the chimeric
709 gene *Quetzalcoatl* in *Drosophila melanogaster*. *Proc. Natl. Acad. Sci. U. S. A.* 107:
710 10943–10948.
- 711 Rousselle M., M. Mollion, B. Nabholz, T. Bataillon, and N. Galtier, 2018 Overestimation of the
712 adaptive substitution rate in fluctuating populations. *Biol. Lett.* 14.
713 <https://doi.org/10.1098/rsbl.2018.0055>
- 714 Schrider D. R., and A. D. Kern, 2018 Supervised Machine Learning for Population Genetics: A
715 New Paradigm. *Trends Genet.* 34: 301–312.
- 716 Slatkin M., 1996 Gene genealogies within mutant allelic classes. *Genetics* 143: 579–587.
- 717 Sousa V., S. Peischl, and L. Excoffier, 2014 Impact of range expansions on current human
718 genomic diversity. *Curr. Opin. Genet. Dev.* 29: 22–30.
- 719 Tajima F., 1990 Relationship between DNA polymorphism and fixation time. *Genetics* 125:
720 447–454.

- 721 Tavaré S., 1984 Line-of-descent and genealogical processes, and their applications in population
722 genetics models. *Theor. Popul. Biol.* 26: 119–164.
- 723 Teshima K. M., G. Coop, and M. Przeworski, 2006 How reliable are empirical genomic scans for
724 selective sweeps? *Genome Res.* 16: 702–712.
- 725 Thornton K. R., and J. D. Jensen, 2007 Controlling the false-positive rate in multilocus genome
726 scans for selection. *Genetics* 175: 737–750.
- 727 Wares J. P., 2009 Evolutionary dynamics of transferrin in *Notropis*. *J. Fish Biol.* 74: 1056–1069.
- 728 Weissman D. B., and N. H. Barton, 2012 Limits to the rate of adaptive substitution in sexual
729 populations. *PLoS Genet.* 8: e1002740.
- 730 Zhao L., M. Lascoux, A. D. J. Overall, and D. Waxman, 2013 The characteristic trajectory of a
731 fixing allele: a consequence of fictitious selection that arises from conditioning. *Genetics*
732 195: 993–1006.